Chinese Journal of Natural Medicines

New tetrahydroanthraquinones and γ-butenolides from the fungus *Auxarthron umbrinum* DSM3193

Ling Tian, Bingyu Liu, Qian Wei, Chen Zhang, Jiamin Shang, Xiaoxue Li, Xiuying Yang, Jinhua Wang, Youcai Hu

Citation: Ling Tian, Bingyu Liu, Qian Wei, Chen Zhang, Jiamin Shang, Xiaoxue Li, Xiuying Yang, Jinhua Wang, Youcai Hu, New tetrahydroanthraquinones and γ-butenolides from the fungus *Auxarthron umbrinum* DSM3193, Chinese Journal of Natural Medicines, 2025, 23(8), 951-960. doi: 10.1016/S1875-5364(25)60930-7.

View online: https://doi.org/10.1016/S1875-5364(25)60930-7

Chinese Journal of Natural Medicines 23 (2025) 951-960

Contents lists available at ScienceDirect

Chinese Journal of Natural Medicines

journal homepage: www.cjnmcpu.com/

Original article

New tetrahydroanthraquinones and γ-butenolides from the fungus *Auxarthron umbrinum* DSM3193

Ling Tian, Bingyu Liu, Qian Wei, Chen Zhang, Jiamin Shang, Xiaoxue Li, Xiuying Yang, Jinhua Wang, Youcai Hu*

State Key Laboratory of Bioactive Substance and Function of Natural Medicines, Institute of Materia Medica, Chinese Academy of Medical Sciences & Peking Union Medical College, Beijing 100050, China

ARTICLE INFO

Article history:
Received 10 August 2024
Revised 28 November 2024
Accepted 14 January 2025
Available online 20 August 2025

Keywords:
Auxarthron umbrinum
One strain many compounds (OSMAC)
Tetrahydroanthraquinone
γ-Butenolide
Cytotoxicity
Fibroblast proliferation

ABSTRACT

Nine novel compounds, comprising seven tetrahydroanthraquinones (auxarthrolones A–G, **1**–**7**), a γ-butenolide glycoside (malfilamentoside E, **26**), and a γ-butenolide (auxarthrolide A, **27**), together with eighteen known compounds (**8**–**25**) were isolated from rice-based solid culture of *Auxarthron umbrinum* (*A. umbrinum*) DSM3193 using the one strain many compounds (OSMAC) approach. The structural elucidation of these compounds was accomplished through nuclear magnetic resonance (NMR), mass spectrometry (MS), and NMR calculation combined with DP4+ analysis or MAEΔΔδ parameter, while the absolute configurations of new compounds were established through single-crystal X-ray diffraction, electronic circular dichroism (ECD) spectroscopic data analysis and/or chemical derivatization. Austrocortilutein (**10**) and auxarthrol H (**14**) demonstrated moderate cytotoxicity against U87 and U251 [half maximal inhibitory concentration (IC_{50}) 3.5–12.1 μmol·L^{-1}]. Additionally, auxarthrolone A (**1**), auxarthrol H (**14**), eupolyphagin B (**15**), and 7-hydroxy-2-(2-hydroxypropyl)-5-methylchromone (**17**) exhibited torsional effects on fibroblast proliferation challenges induced by oleic acid, thus demonstrating fibroblast proliferation-promoting activity.

1. Introduction

Fungal natural products exemplified by penicillin G, lovastatin, and cyclosporine have attracted significant attention due to their complex structures and profound biological activities [1-3]. The fungus *Auxarthron umbrinum* (*A. umbrinum*) has been notable as a producer of diverse natural products, exhibiting significant bioactivities, including anti-HIV [4], cytotoxicity [5-7], inhibitory activity of cannabinoid CB1 receptor [8], and α-glucosidase inhibition [9]. In our previous study, the whole genome of *A. umbrinum* DSM3193 was sequenced [4], revealing the presence of substantially more biosynthetic gene clusters for natural products than compounds previously isolated from it [10-12]. This finding suggests numerous undiscovered secondary metabolites. Therefore, further investigation of the secondary metabolites of *A. umbrinum* remains essential.

Many putative gene clusters demonstrate limited expression under laboratory conditions, significantly impeding the discovery of compounds with novel structures and functionalities [13-14]. Modifying the growth conditions of microorganisms can yield various secondary metabolites; consequently, the one strain many compounds (OSMAC) approach has been widely employed in the discovery of new natural products [15, 16]. In this study, *A. umbrinum* was cultivated using different media, including potato dextrose agar (PDA), malt medium, and rice medium. LC analysis of metabolites across different media revealed the highest metabolite richness from *A. umbrinum* grown on a rice-based solid medium (Fig. S1). Systematic chemical investigation resulted in the isolation and characterization of twenty-seven compounds, including nine new ones (**1**–**7**, **26** and **27**) from the metabolites of rice medium (Fig. 1). All compounds underwent assessment for their cytotoxicity and activity in promoting fibroblast proliferation. This paper describes the isolation, structure elucidation, and biological evaluation of compounds **1**–**27**.

2. Results and discussion

2.1. Identification and structural elucidation

Auxarthrolone A (**1**) was isolated as a colorless crystal. Its molecular formula was established as $C_{18}H_{20}O_{10}$ through high-resolution electrospray ionization mass spectrometry (HR-ESI-MS) (*m/z* 397.1134 [M + H]$^+$, Calcd. 397.1130), indicating 9 degrees of unsaturation. Analysis of 1D nuclear magnetic resonance (NMR) data of **1** (Tables 1 and 2) revealed a structure closely related to auxarthrol B (**9**) [17]. Compound **1** was distinguished from **9** by the presence of an additional methyl (δ_C 21.0, C-14; δ_H 1.81, H-14) and an ester carbonyl (δ_C 169.5, C-13) in **1**, suggesting that **1** represented the acetylated derivative of **9**. The heteronuclear multiple bond correlation (HMBC) from H-14 to C-9a confirmed the acetoxyl group's position at C-9a (Fig. 2). The relative config-

* Corresponding author.
E-mail address: huyoucai@imm.ac.cn

https://doi.org/10.1016/S1875-5364(25)60930-7

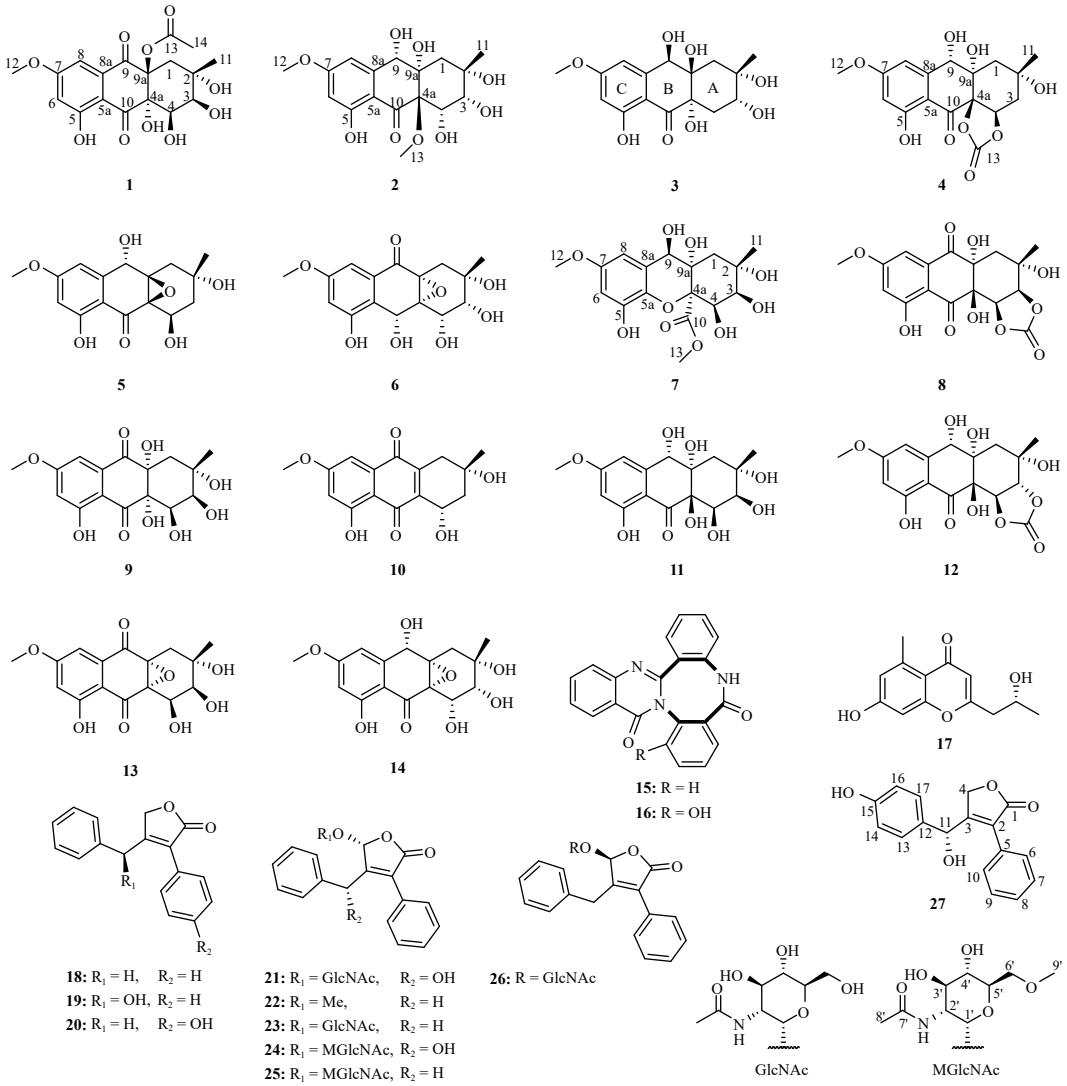

Fig. 1 Structures of compounds **1**–**27** isolated from *A. umbrinum* DSM3193.

uration of C-2, C-3 and C-4 was established as 2*S**,3*S**,4*R** based on the small value of $J_{3\text{-}4}$ (3.1 Hz) and nuclear Overhauser effect spectroscopy (NOESY) correlation from H-3 to H-4, and from 4-OH to H-11 (Fig. 3). The relative configuration of C-4a and C-9a remained unassigned due to the absence of NOESY correlations, suggesting four possible relative configurations for **1** (Fig. S2). The ^{13}C NMR calculation at the PW1PW91/6-31 + G(d, p)// B3LYP/6-31G(d) level with the PCM solvent model in acetone was utilized to determine the relative configuration of **1**. The calculated carbon chemical shifts for **1a** demonstrated the highest correlation with experimental values, showing the smallest mean absolute deviation (MAD, **1a**: 1.7450 *vs* **1b**–**1d**: 3.0989, 2.7828, and 2.1830, respectively) and corrected mean absolute deviation (CMAD, **1a**: 1.5562 *vs* **1b**–**1d**: 2.7447, 2.4871, and 1.6780, respectively) values (Tables S1 and S2). Furthermore, DP4+ analysis based on ^{13}C NMR data indicated 97.56% probability for isomer **1a** (Fig. S3), establishing supporting the 2*S**,3*S**,4*R**,4a*S**,9a*S** relative configuration of **1**. The absolute configuration of **1** was determined through electronic circular dichroism (ECD) calculations of the two possible enantiomers, (2*S*,3*S*,4*R*,4a*S*,9a*S*)-**1** and (2*R*,3*R*,4*S*,4a*R*,9a*R*)-**1**. The calculated ECD spectrum of (2*S*,3*S*,4*R*,4a*S*,9a*S*)-**1** aligned well with the experimental ECD spectrum of **1** (Fig. S4), establishing the absolute configuration of **1** as 2*S*,3*S*,4*R*,4a*S*,9a*S*. This configuration was subsequently confirmed through single-crystal X-ray diffraction analysis of **1** (Fig. 4).

Auxarthrolone B (**2**), a yellow solid, exhibited a molecular formula of $C_{17}H_{22}O_9$ as determined by HR-ESI-MS at *m/z* 371.1340 $[M + H]^+$ (Calcd. 371.1337), which was 14 Da greater than auxarthrol E (**11**) [18]. The ^{1}H NMR (Table 1) and ^{13}C NMR (Table 2) spectra of **2** demonstrated high similarity to those of **11**, with the primary difference being additional methoxyl signals (δ_C 57.1, C-13; δ_H 3.51, H-13) in **2**. These findings indicated that **2** represented a methylated derivative of **11**. The HMBC from H-13 to C-4a (δ_C 82.7) enabled the assignment of the methoxyl group at C-4a (Fig. 2). The relative configuration of C-2, C-3, C-4, and C-4a was established as 2*R**,3*S**,4*R**,4a*S** based on the small value of $J_{3\text{-}4}$ (4.6 Hz) and the NOESY correlations of H-3 with H-11/H-13/H-4 (Fig. 3). To confirm the relative configuration of **2**, theoretical calculations of ^{13}C NMR data for the four possible isomers **2a**–**2d** (Fig. S5) were conducted. The relative configuration of (2*S**,3*R**,4*S**,4a*R**,9*S**,9a*S**)-**2** was determined through computational ^{13}C NMR analysis with DP4+ probability analysis showing 100% probability (Fig. S6, Tables S3 and S4). ECD calculation was utilized to determine the absolute configuration of **2**. The calculated ECD spectra of two stereoisomers, (2*S*,3*R*,4*S*,4a*R*,9*S*,9a*S*)-**2** and (2*R*,3*S*,4*R*,4a*S*,9*R*,9a*R*)-**2**, were compared with the experimental ECD spectrum. The calculated ECD spectrum of (2*S*,3*R*,4*S*,4a*R*,9*S*,9a*S*)-**2** matched the experimental ECD spectrum precisely (Fig. S4), thus confirming the absolute configuration of **2** as 2*S*,3*R*,4*S*,4a*R*,9*S*,9a*S*.

Auxarthrolone C (**3**) was isolated as a yellow solid with a molecular formula of $C_{16}H_{20}O_8$ based on its HR-ESI-MS data (*m/z*

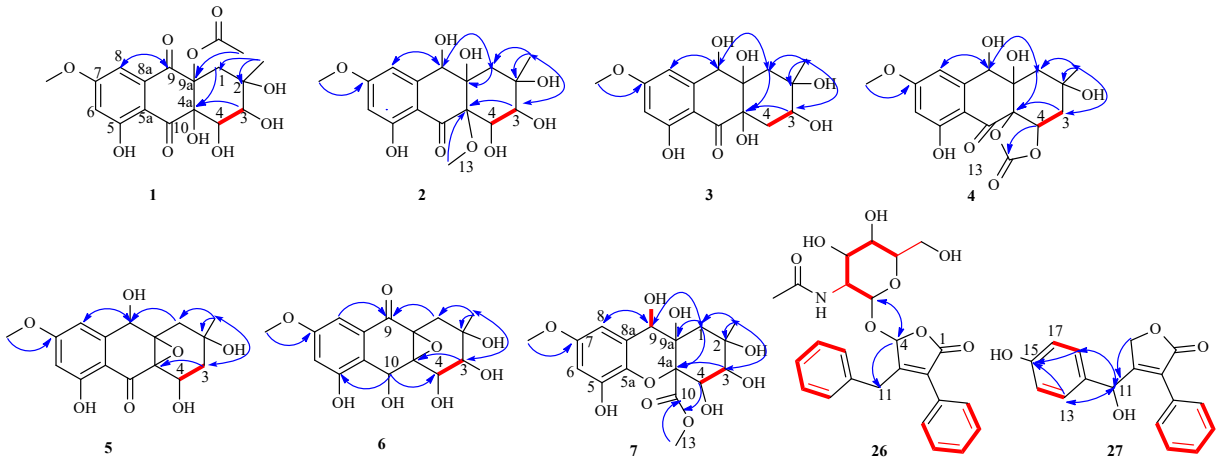

Fig. 2 Key ^{1}H–^{1}H COSY (red) and HMBC (blue) correlations of compounds **1**–**7**, **26** and **27**.

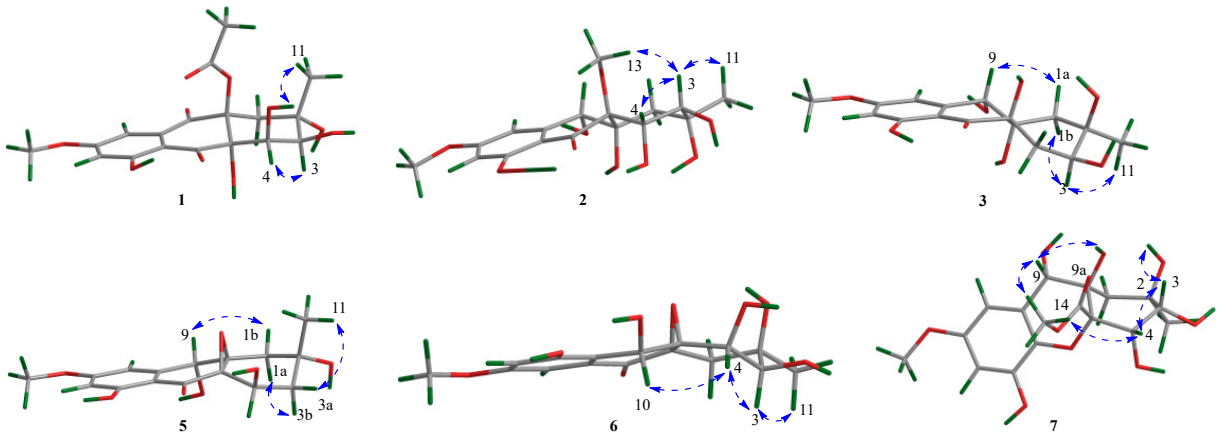

Fig. 3 Key NOESY (Blue) correlations of compounds **1**–**3** and **5**–**7**.

341.1236 [M + H]$^{+}$, Calcd. 341.1231), containing one less oxygen atom than auxarthrol E (**11**) [18]. The 1D NMR spectra of **3** (Tables 1 and 2) and **11** exhibited nearly identical patterns, except for the presence of a methylene (δ_C 28.3, C-4; δ_H 2.41/2.47, H-4) in **3** instead of an oxygenated methine in **11**. The ^{1}H–^{1}H correlation spectroscopy (COSY) correlation of H-3 (δ_H 3.63) with H_2-4 (Fig. 2) indicated that C-4 was deoxygenated. The relative configuration of C-2, C-3, and C-9 was determined as 2*S**,3*R**,9*R** through the NOESY correlation of H-11 with H-3/H-1b, and H-9 with H-1a (Fig. 3). The relative configuration of **3** at C-4a and C-9a remained unresolved, suggesting four possible relative configurations for **3** (Fig. S7). These configurations underwent ^{13}C NMR shift calculations and DP4+ probability analysis (99.99% for 2*S**, 3*R**,4a*S**,9*R**,9a*R** configurations) (Fig. S8, Tables S5 and S6). To establish the absolute configuration of **3**, two stereoisomers, (2*S*,3*R*,4a*S*,9*R*,9a*R*)-**3** and (2*R*,3*S*,4a*R*,9*S*,9a*S*)-**3**, were subjected to ECD calculation. The calculated ECD spectrum of (2*S*,3*R*, 4a*S*,9*R*,9a*R*)-**3** matched the experimental spectrum (Fig. S4).

Auxarthrolone D (**4**) was obtained as a light-yellow crystal. Its molecular formula was established as $C_{17}H_{18}O_9$ through HR-ESI-MS analysis (*m*/*z* 367.1026 [M + H]$^{+}$, Calcd. 367.1024). The 1D NMR spectra (Tables 1 and 2) indicated **4** as a homolog of **3**, with the primary difference being an additional carbonate group (δ_C 153.3, C-13) [19] in **4**. The HMBC from H-4 (δ_H 5.57) to C-13 and the deshielded C-4a at δ_C 83.7 ($\Delta\delta_C$ +21) revealed that the carbonate group was positioned at C-4 and C-4a (Fig. 2). The ^{1}H–^{1}H COSY correlations between H-3 (δ_H 1.88/2.69) and H-4 confirmed C-3 rather than C-4 as a methylene in **4** (Fig. 2). The absolute configuration of **4** was determined through single-crystal X-ray diffraction analysis, yielding a Flack parameter of −0.10 (13) using Cu Kα radiation. This analysis established the absolute configuration of **4** as 2*R*,4*R*,4a*R*,9*S*,9a*S* (Fig. 4).

Auxarthrolone E (**5**) was isolated as a yellow solid, exhibiting an [M + H]$^{+}$ peak at *m*/*z* 323.1127 (Calcd. 323.1126) in HR-ESI-MS, corresponding to the molecular formula $C_{16}H_{18}O_7$ for **5**. The 1D NMR spectra (Tables 2 and 3) of **5** showed close similarity to those of auxarthrol H (**14**) [18]. The primary distinction was the substitution of an oxygenated methine in **14** with a methylene (δ_C 42.1, C-3; δ_H 1.82 and 1.92, H-3) in **5**. The ^{1}H–^{1}H COSY correlations between H_2-3 and H-4 (δ_H 4.84) confirmed the methylene position at C-3 (Fig. 2). The relative configuration of C-2 and C-9 was established as 2*R**,9*S** through NOESY correlations of H-11 with H_a-3, H_b-3 with H_a-1, and H_b-1 with H-9 (Fig. 3). The relative configuration of C-4 and C-2 was determined by analyzing the dihedral angle dependence of $J_{4\text{-}3a}$ and $J_{4\text{-}3b}$ values in two possible configurations (2*R**,4*R** and 2*R**,4*S**) [20]. The analysis revealed that the values of $J_{4\text{-}3a}$ and $J_{4\text{-}3b}$ aligned closely with $J_{4\text{-}3a}$ (2.9 Hz) and $J_{4\text{-}3b}$ (4.4 Hz) when the relative configuration was 2*R**,4*R** (Fig. S9). Consequently, the relative configuration of **5** was determined as 2*R**,4*R**,9*S**. Since the relative configuration at C-4a and C-9a remained undetermined, two candidate relative configurations were proposed for **5** (Fig. S10). To resolve this, two diastereomers, **5a** and **5b**, underwent NMR calculation. DP4+ analysis (100% for 2*R**,4*R**,4a*R**,9*S**,9a*R**) established the relative configuration of **5** (Fig. S11, Tables S7–S9). The absolute configuration of **5** was determined as 2*R*,4*R*,4a*R*,9*S*,9a*R* through comparison of experimental and calculated ECD spectra (Fig. S4).

Auxarthrolone F (**6**), isolated as a light red solid, exhibited a

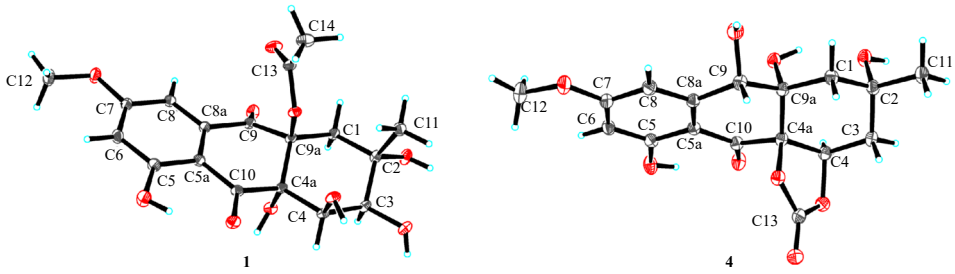

Fig. 4 The ORTEP diagrams of compounds **1** and **4** (displacement ellipsoids are drawn at the 30% probability level).

Table 1 ^{1}H NMR data of compounds **1**–**4**.

No.	**1**[ad] δ_H, mult. (*J* in Hz)	**2**[ae] δ_H, mult. (*J* in Hz)	**3**[ae] δ_H, mult. (*J* in Hz)	**4**[ad] δ_H, mult. (*J* in Hz)
1	2.49, d (15.3) 2.56, d (15.3)	2.02, dd (14.6, 1.4) 2.14, d (14.6)	2.37, ovl [c] 2.45, ovl [c]	2.01, d (14.9) 2.40, dd (14.9, 2.2)
3	3.95, ovl [c]	3.75, t (4.6)	3.63, t (5.8)	1.88, dd (14.4, 8.7) 2.69, m
4	4.57, d (3.1)	4.77, ovl [c]	2.41, ovl [c] 2.47, ovl [c]	5.57, dd (8.7, 2.69)
6	6.71, d (2.5)	6.38, d (2.4)	6.38, d (2.6)	6.42, d (2.5)
8	6.82, d (2.5)	6.78, m	6.80, d (2.6, 1.3)	6.83, dd (2.5, 1.1)
9		4.77, ovl [c]	4.95, d (6.8)	4.76, br s
11	1.43, s	1.37, s	1.22, s	1.45, s
12	3.95, ovl [c]	3.90, s	3.88, s	3.91, s
13		3.51, s		
14	1.81, s			
3-OH		3.62, d (6.3)		
4-OH	4.02, s			
5-OH	11.85, s	11.96, s	11.90, s	11.59, s
9-OH			5.29, d (9.2)	

[a] Acetone-d_6; ovl [c] Overlapped; [d] 700 MHz; [e] 600 MHz.

molecular formula of $C_{16}H_{18}O_8$ based on HR-ESI-MS analysis showing an ion at *m/z* 339.1074 $[M + H]^+$ (Calcd. 339.1075), indicating **8** degrees of unsaturation. The 1D NMR spectra of **6** revealed a tetrahydroanthraquinone skeleton analogous to **2**, with the notable distinction being the absence of a methoxy group in **6** (Tables 2 and 3). The HMBC from H-8 (δ_H 6.92) to C-9 (δ_C 192.9) and from H-10 (δ_H 5.76) to C-5 (δ_C 159.4) indicated that C-8a (δ_C 131.1), C-5a (δ_C 118.0) connected to C-9 and C-10 (δ_C 67.1), respectively (Fig. 2). The upfield shifts of C-4a (δ_C 65.3) and C-9a (δ_C 65.2) in **6** compared to **2** suggested the presence of an epoxide ring, consistent with the HR-ESI-MS data indicating **8** degrees of unsaturation. The relative configuration of C-2, C-3, C-4 and C-10 was established as 2R^*,3S^*,4R^*,10S^* based on the small coupling constant $J_{3\text{-}4}$ (3.6 Hz) and NOESY correlations between H-10 and H-4, and H-11 with H-3 (Fig. 3). The undetermined relative configuration of C-4a/C-9a led to two possible relative configurations for **6** (Fig. S12). To resolve this, ^{13}C NMR chemical shifts of **6a** and **6b** were calculated using mPW1PW91/6-31G + (d, p) with PCM solvent model in acetone. The calculations for **6a** (R^2 = 0.9972) showed better correlation with experimental data than **6b** (R^2 = 0.9940) (Table S10), and DP4+ analysis confirmed **6a** with 100% probability match to experimental ^{13}C NMR data (Fig. S96 and Table S11), establishing **6a** as the correct relative configuration. The absolute configuration of **6** was determined by comparing experimental and calculated ECD spectra of (2*S*,3*R*,4*S*,4a*S*,9a*R*,10*R*)-**6** and (2*R*,3*S*,4*R*,4a*R*,9a*S*,10*S*)-**6**, respectively. The calculated ECD spectrum of (2*S*,3*R*,4*S*,4a*S*,9a*R*,10*R*)-**6** at B3LYP/6-31 + G(d) level matched the experimental spectrum (Fig. S4), confirming the absolute configuration as 2*S*,3*R*,4*S*,4a*S*,9a*R*,10*R*.

Auxarthrolone G (**7**) was isolated as a yellow solid with a molecular formula of $C_{17}H_{22}O_{10}$, determined by the HR-ESI-MS ion at *m/z* 409.1105 $[M + Na]^+$ (Calcd. 409.1106), indicating **7** degrees of unsaturation. The 1D NMR spectra of **7** exhibited similarities to those of **2**, suggesting the presence of A-ring (Tables 2 and 3). The ^{1}H NMR and ^{13}C NMR spectra of **7** revealed two methoxy moieties at δ_H 3.60 (H-13) and 3.70 (H-12), and an ester carbonyl (δ_C 171.9, C-10). The HMBC correlations (Fig. 3) from H-13 to C-10 indicated the presence of the methoxyacetyl group. Based on the HMBC from H-4 (δ_H 4.66) to C-10, the methoxyacetyl group was positioned at C-4a. The ^{1}H NMR resonance of two *meta*-coupled aromatic protons (δ_H 6.39, d, *J* = 3.0 Hz, H-6; 6.30, d, *J* = 3.0 Hz, H-8) and the ^{13}C NMR resonance at δ_C 147.2 (C-5), 134.5 (C-5a), 103.5 (C-6), 155.4 (C-7), 105.6 (C-8), and 124.1 (C-8a) indicated a tetrasubstituted benzene ring. The HMBCs from H-12 to C-7 confirmed the location of the methoxy group at C-7. The ^{1}H NMR resonance at δ_H 8.28 (s, 5-OH), 4.88 (br s, 9-OH), and 5.11 (s, 9a-OH) indicated a phenolic hydroxyl group and two alcoholic hydroxyl groups. The HMBCs (Fig. 2) of H-8 with C-9, and H-1 with C-9a/C-9 demonstrated that C-9 was connected to C-8a of a benzene ring and C-9a of A-ring. The remaining hydroxyl group (δ_H 8.28, s, 5-OH) and ethereal oxygen atom were assigned to C-5 and C-5a/C-4a, respectively, through comparison with the chemical shifts of C-5a and C-5 in reported 9-dehyroxyeurotinone [21]. The relative configuration of **7** was established as 2R^*,3R^*,4S^*,4aS^*,9S^*,9aR^* based on the small value of $J_{3\text{-}4}$ (3.6 Hz) and the NOESY correlations of 2-OH with H-3, H-3 with H-4, H-13 with H-4/H-9, and 9a-OH with H-9 (Fig. 3). To determine the absolute configuration of **7**, theoretical ECD spectra were calculated for two possible isomers, (2*S*,3*S*,4*R*,4a*R*,9*R*,9a*S*)-**7** and (2*R*,3*R*,4*S*,4a*S*,9*S*,9a*R*)-**7**. The theoretical data for (2*S*,3*S*,4*R*,4a*R*,9*R*,9a*S*)-**7** closely matched the experimental ECD spectrum (Fig. S4), confirming the absolute configuration of **7** as 2*S*,3*S*,4*R*,4a*R*,9*R*,9a*S*.

Malfilamentoside E (**26**), obtained as a white powder, exhibited a molecular formula of $C_{25}H_{27}NO_8$ based on HR-ESI-MS analysis, showing a peak at *m/z* 470.1821 $[M + H]^+$ (Calcd. 470.1809). The ^{1}H NMR and ^{13}C NMR spectral data of **26** (Table 4) demonstrated similarity to those of malfilamentoside D (**23**) [12]. Analysis of key HMBCs of **26** (Fig. 2) revealed an identical planar structure to that of **23** (Fig. 1). The sugar component of **26** was identified as 2-*N*-acetylamide-D-glucopyranoside through GC-MS analysis (Fig. S14). For determining the absolute configuration at C-4, ECD calculations were performed on two possible epimers, 4*S*-**26** and 4*R*-**26**. The experimental ECD spectrum of **26** and calculated ECD spectrum of 4*S*-**26** both displayed a negative Cotton effect near 250 nm (Fig. S15), establishing the C-4 absolute configuration in **26** as 4*S*. This configuration was further supported by ^{13}C NMR calculations (Table S12), the MAE$\Delta\Delta\delta$ parameter for comparing experimental and calculated data [22], and literature comparison [12]. The calcd_26b calcd_26a/exptl_23 exptl_26 alignment demonstrated the lowest MAE$\Delta\Delta\delta$ values among possible comparisons (Fig. S16).

Auxarthrolide A (**27**), isolated as a yellow solid, possessed a molecular formula of $C_{17}H_{14}O_4$ based on HR-ESI-MS analysis

Table 2 ^{13}C NMR data for compounds **1**–**7**.

No.	**1**[ad]	**2**[ae]	**3**[ae]	**4**[ad]	**5**[bd]	**6**[ad]	**7**[ae]
1	36.2	35.0	38.3	38.5	42.0	31.6	36.8
2	72.5	75.1	71.1	70.8	68.3	70.4	74.2
3	74.7	78.2	71.1	41.5	42.1	74.4	78.8
4	74.0	69.2	28.3	74.2	64.2	67.4	69.8
4a	79.4	82.7	62.7	83.7	62.6	65.3	83.8
5	165.6	166.0	165.7	166.2	166.5	159.4	147.2
5a	110.3	109.7	107.5	108.6	108.3	118.0	134.5
6	105.9	100.4	100.3	100.5	100.9	108.9	103.5
7	167.4	168.1	167.8	168.3	168.5	161.4	155.4
8	107.4	107.6	106.8	108.1	107.3	103.5	105.6
8a	138.0	148.9	146.3	147.8	146.2	131.1	124.1
9	191.3	70.9	70.2	71.5	70.4	192.9	71.0
9a	86.4	80.1	65.9	75.9	65.5	65.2	75.4
10	199.6	203.1	198.4	194.4	198.3	67.1	171.9
11	24.1	27.5	23.3	30.9	31.8	26.9	27.1
12	56.7	56.2	56.2	56.3	56.2	55.7	55.7
13	169.5	57.1		153.3			52.7
14	21.0						

[a] Acetone-d_6; [b] Methanol-d_4; [d] 175 MHz; [e] 150 MHz.

Table 3 ^{1}H NMR data of compounds **5**–**7**.

No.	**5**[bd] δ_H, mult. (*J* in Hz)	**6**[ad] δ_H, mult. (*J* in Hz)	**7**[ae] δ_H, mult. (*J* in Hz)
1	2.37, dd (15.2, 1.5) 2.46, d (15.2)	2.58, d (15.8) 2.07, ovl [c]	1.47, d (14.8) 1.84, d (14.8)
3	1.82, ddd (14.2, 2.9, 1.5) 1.92, dd (14.2, 4.4)	3.67, d (3.6)	3.65, m
4	4.84, dd (4.4, 2.9)	4.60, d (3.6)	4.66, m
6	6.40, d (2.5)	6.65, d (2.7)	6.39, d (3.0)
8	6.76, dd (2.5, 1.3)	6.92, d (2.7)	6.30, d (3.0)
9	4.86, (1.3)		4.27, br s
10		5.76, s	
11	1.39, s	1.29, s	1.18, s
12	3.86, s	3.80, s	3.70 s
13			3.60, s
2-OH			4.98, s
5-OH			8.28, s
9-OH			4.88, br s
9a-OH			5.11, s

[a] Acetone-d_6; [b] Methanol-d_4; ovl [c] Overlapped; [d] Recorded at 700 MHz; [e] Recorded at 600 MHz.

showing an ion at *m/z* 283.0971 $[M + H]^+$ (Calcd. 283.0965), exceeding gotjawalide (**19**) [23] by 16 Da. The 1D NMR data (Table 4) of **27** showed similarity to **19**, with the primary distinction being the absence of one aromatic proton. This indicated that **27** represented a hydroxylated variant of **19** (Fig. 1). HMBCs (Fig. 2) from H-11 to C-13/C-17, H-13 to C-11/C-15, and H-17 to C-11/C-15 indicated hydroxyl substitution at C-15. ECD calculations determined the absolute configuration of **27**, with the experimental ECD spectrum of **27** matching the calculated spectrum of 11*S*-**27** (Fig. S15), confirming the 11*S* absolute configuration.

The known compounds isolated from *A. umbrinum* were identified as ocauxarthrol A (**8**) [10], auxarthrol B (**9**) [17], austrocortilutein (**10**) [24], auxarthrol E (**11**) [18], chrysoqueen (**12**) [19], auxarthrol A (**13**) [5], auxarthrol H (**14**) [18], eupolyphagin B (**15**) [9], eupolyphagin (**16**) [25], 7-hydroxy-2-(2-hydroxypropyl)-5-methylchromone (**17**) [26], gymnoascolide A (**18**) [27], gotjawalide (**19**) [23], eutypoid A (**20**) [28], gotjawaside (**21**) [23], 4-benzyl-5-methoxy-3-phenylfuranone (**22**) [29], malfilamentoside D (**23**) [12], malfilamentoside B (**24**), and malfilamentoside A (**25**) [30]. Structural identification of these compounds was accomplished by comparing their NMR spectroscopic data with those previously reported in the literature.

2.2. Cytotoxicity

The isolated tetrahydroanthraquinones were evaluated for their cytotoxic activity against U87 and U251 cell lines. Compounds **10** and **14** exhibited cytotoxicity against U87 cells with IC_{50} values of 3.4 and 9.4 μmol·L^{-1}, and U251 cells with IC_{50} values of 9.5 and 12.1 μmol·L^{-1}, respectively (Fig. S17).

2.3. Fibroblast proliferation activity

The fibroblast proliferation activity of compounds **1**–**27** was evaluated using the NIH3T3 cell line. The NIH3T3 cells were incubated with high concentration oleic acid (0.2 mmol·L^{-1}). Compared to the normal blank, compounds **1**, **14**, **15**, and **17** demonstrated significant effects on cell proliferation challenges induced by oleic acid (Fig. 5). Consequently, compounds **1**, **14**, **15**, and **17** were determined to possess fibroblast proliferation properties.

Table 4 ^{1}H NMR and ^{13}C NMR data of compounds **26** and **27**.

No.	**26** (in acetone-d_6) [a]		**26** (in DMSO-d_6) [b]		**27** (in methanol-d_4) [b]	
	δ_H, mult. (J in Hz)	δ_C	δ_H, mult. (J in Hz)	δ_C	δ_H, mult. (J in Hz)	δ_C
1		170.5		169.6		175.6
2		131.5		135.8		131.2
3		157.5		156.6		166.0
4	6.05, s	98.2	6.02, s	97.3	4.92, dd (18.2, 1.0) 5.14, d (18.2)	70.9
5		130.3		130.0		127.4
6	7.56, ovl [c]	129.9	7.29, m	128.6	7.42, ovl [c]	130.2
7	7.49, ovl [c]	129.4	7.47, ovl [c]	128.7	7.42, ovl [c]	129.5
8	7.46, m	130.0	7.44, ovl [c]	129.0	7.42, ovl [c]	129.8
9	7.49, ovl [c]	129.4	7.29, ovl [c]	128.6	7.42, ovl [c]	129.5
10	7.56, ovl [c]	129.9	7.47, ovl [c]	128.7	7.42, ovl [c]	130.2
11	3.87, d (15.7) 4.16, d (15.7)	33.0	3.76, d (15.7) 4.05, d (15.7)	31.6	5.83, s	70.0
12		137.2				133.0
13	7.31, ovl [c]	129.7	7.23, ovl [c]	128.5	7.12, ovl [c]	128.5
14	7.32, ovl [c]	129.8	7.47, ovl [c]	128.5	6.74, ovl [c]	116.5
15	7.25, ovl [c]	127.8	7.23, ovl [c]	126.7		158.6
16	7.32, ovl [c]	129.8	7.47, ovl [c]	128.5	6.74, ovl [c]	116.5
17	7.31, ovl [c]	129.7	7.23, ovl [c]	128.5	7.12, ovl [c]	128.5
1′	5.24, d (3.7)	97.7	5.10, d (3.7)	96.4		
2′	3.98, m	54.4	3.72, ddt (12.4, 8.1, 4.0)	53.2		
3′	3.63, m	72.3	3.47, m	69.8		
4′	3.52, m	71.7	3.26, m	69.6		
5′	3.46, m	74.6	3.28, m	73.7		
6′	3.51, m 3.61, m	61.9	3.22, m 3.43, m	59.9		
7′		170.8		169.7		
8′	1.90, s	22.9	1.85, s	22.5		
2′-NH	7.07, d (8.4)		7.86, d (8.0)			

[a] ^{1}H NMR (600 MHz), ^{13}C NMR (150 MHz); [b] ^{1}H NMR (700 MHz), ^{13}C NMR (175 MHz); ovl [c] Overlapped.

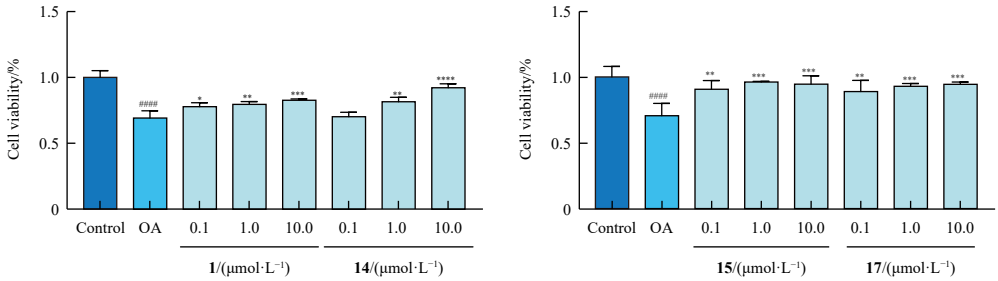

Fig. 5 Fibroblast proliferation of compounds **1**, **14**, **15** and **17** (0, 0.1, 1.0, 10.0 μmol·L^{-1}) assayed on NIH3T3 cells incubated with high concentration (0.2 mmol·L^{-1}) oleic acid. Cell viability was tested by the CCK8 method. Control group: NIH3T3 cells were incubated with a serum-free medium; OA group: NIH3T3 cells were incubated with a serum-free medium containing 0.2 mmol·L^{-1} oleic acid; Treatment group: NIH3T3 cells were incubated with a serum-free medium containing 0.2 mmol·L^{-1} oleic acid and various concentration of compounds. The data are presented as mean ± SD (n = 3). $^{**}P < 0.01$, $^{***}P < 0.001$, $^{****}P < 0.0001$ *vs* Control.

3. Experimental

3.1. General experimental procedures

HR-ESI-MS data were obtained either a Q-Exactive Focus LC/MS system (Thermo Fisher Scientific, USA) or a 1260 Infinity II UPLC coupled to a 6500 quadrupole time-of-flight (Q-TOF) mass spectrometer (Agilent Technologies Inc., Santa Clara, CA, USA). Infrared (IR) spectra were recorded using a Nicolet 5700 FT-IR spectrometer equipped with a transmission microscope (Thermo Fisher Scientific, USA). Optical rotations were meas-

ured on an Autopol IV automatic polarimeter (Rudolph Research Co., USA). Ultraviolet (UV) absorption spectra were obtained on a JASCO V-650 spectrophotometer, while electronic circular dichroism (ECD) spectra were recorded in methanol using a JASCO J-815 spectropolarimeter (JASCO, Japan). NMR spectra were recorded on an Agilent 700 MHz spectrometer (Agilent Technologies Inc., Santa Clara, CA, USA) and a Bruker AVANCE III HD 600 MHz spectrometer (Bruker, Germany). Samples were dissolved in CD_3OD, DMSO-d_6, or acetone-d_6, with tetramethylsilane (TMS; Cambridge Isotope Laboratories, Inc., USA) used as the internal standard. Silica gel (Qingdao Haiyang Chemical Co., Ltd., Qingdao, China), ODS (50 μm, YMC, Kyoto, Japan), and Sephadex LH-20 (Pharmacia Biotech AB, Uppsala, Sweden) were utilized for CC. For chromatographic separation, silica gel (Qingdao Haiyang Chemical Co., Ltd., Qingdao, China), reversed-phase ODS (50 μm, YMC, Kyoto, Japan), and Sephadex LH-20 gel (Pharmacia Biotech AB, Uppsala, Sweden) were employed for column chromatography. Semipreparative high-performance liquid chromatography (HPLC) was performed using a LabAlliance Series III pump with a model 201 UV detector (Beijing Xianming Leshi Technology Development Co., Ltd., Beijing, China), and a YMC-Pack ODS-A column (250 mm × 10 mm, 5 μm; YMC, Kyoto, Japan). Analytical HPLC was carried out on a Waters ACQUITY H-Class UPLC system equipped with a QDA mass detector and a BEH C_{18} column (1.7 μm, 50 mm × 2.1 mm; Waters Technologies, Shanghai, China). Compound concentration and drying were performed using a JM.CV600 freeze centrifugal concentrator (JM, Beijing, China).

3.2. Biological material

Dulbecco's modified Eagle medium (DMEM) was obtained from Gibco (USA). Antibiotics were acquired from Solarbio (China). Oleic acid was procured from Sigma (USA). 96-Well plates were obtained from Corning (USA). Cell Counting Kit-8 was purchased from Meilunbio (China). U87-MG and U251-MG were acquired from the American Type Culture Collection (ATCC, Manassas, VA, USA). The NIH3T3 cell line was obtained from the Cell Resource Center, Institute of Basic Medicine, Chinese Academy of Medical Sciences. Fetal Bovine Serum was procured from Gibco (New Zealand).

3.3. Fungal material

A. umbrinum DSM3193 was obtained from China Center of Industrial Culture Collection and maintained in Prof. Youcai Hu's laboratory at the State Key Laboratory of Bioactive Substance and Function of Natural Medicines, Institute of Materia Medica, Chinese Academy of Medical Sciences & Peking Union Medical College.

3.4. Fermentation, extraction, and isolation

A. umbrinum was cultivated on PDA medium (BD, Franklin Lakes, NJ, USA) at 28 °C for 4 d. Seed culture of the fungus was prepared using agar plugs (0.5 cm^3), which were inoculated in potato-dextrose broth (BD, Franklin Lakes, NJ, USA) medium and incubated at room temperature for 7 d at 180 $r{\cdot}min^{-1}$. Subsequently, the fungus was grown in fifty 500 mL Fernbach flasks containing rice medium (100.00 g rice and 100.0 mL of H_2O each). After incubation for 25 d, the flask contents were extracted thoroughly with 10 L of ethyl acetate three times. The supernatants were evaporated under reduced pressure to yield an oily extract (42.11 g).

The crude extract was suspended in CH_3OH–H_2O (19∶1) and partitioned with hexane (3 × 3 L). The CH_3OH extraction (Fr. 1, 25.32 g) was subjected to 300–400 mesh silica gel column chromatography, eluting with a gradient of petroleum ether/EtOAc (100∶1 to 0∶100, *V/V*) to afford eleven fractions (Fr. 1A to Fr. 1K).

Fr. 1B (4.32 g) was purified by a Sephadex LH-20 column (CH_3OH/CH_2Cl_2, 2∶1) to yield **18** (3.71 g). Fr. 1D (481.20 mg) was purified by preparative HPLC (CH_3CN/H_2O, 47∶53, 10 $mL{\cdot}min^{-1}$) to obtain **19** (146.16 mg, t_R 22.6 min) and **20** (10.54 mg, t_R 21.0 min).

Fr. 1F (2.60 g) and 1H (415.10 mg) were separated by medium-pressure liquid chromatography (MPLC), respectively, yielding six and four fractions (Fr. 1F1 to Fr. 1F6, Fr. 1H1 to Fr. 1H4). Fr. 1F3 (117.00 mg) was purified by semipreparative HPLC (CH_3CN/H_2O–0.2% FA, 27∶73, 3 $mL{\cdot}min^{-1}$) to yield **9** (10.54 mg, t_R 14.8 min). Fr. 1F4 (20.30 mg) was purified by semipreparative HPLC (CH_3CN/H_2O–0.2% FA, 30∶70, 3 $mL{\cdot}min^{-1}$) to yield **27** (2.01 mg, t_R 14.0 min). Fr. 1F5 (180.10 mg) was purified by HPLC (CH_3CN/H_2O–0.2% FA, 33∶67, 3 $mL{\cdot}min^{-1}$) to yield **8** (133.46 mg, t_R 22.2 min). Fr. 1F6 (43.00 mg) was purified by semipreparative HPLC (CH_3CN/H_2O–0.1% FA, 26∶74, 3 $mL{\cdot}min^{-1}$) to yield **13** (11.77 mg, t_R 19.8 min).

Fr. 1H2 (84.90 mg) was separated by semipreparative HPLC (CH_3OH/H_2O–0.1% FA, 30∶70, 3 $mL{\cdot}min^{-1}$) to obtain **11** (33.55 mg, t_R 17.0 min). Fr. 1H3 (130.50 mg) was separated by semi-preparative HPLC (CH_3CN/H_2O–0.1% FA, 17∶83, 3 $mL{\cdot}min^{-1}$) to obtain **3** (2.43 mg, t_R 30.0 min) and **2** (2.28 mg, t_R 39.2 min). Fr. 1H4 (9.20 mg) was separated by semipreparative HPLC (CH_3CN/H_2O–0.1% FA, 23∶77, 3 $mL{\cdot}min^{-1}$) to obtain **10** (2.23 mg, t_R 25.5 min).

Fr. 1I (3.11 g) was subjected to a Sephadex LH-20 column (CH_3OH) to generate five fractions (Fr. 1I1 to Fr. 1I5). Fr. 1I3 was re-crystallized using CH_3OH to obtain **12** (360.90 mg). Fr. 1J (1.83 g) was fractionated through a Sephadex LH-20 column (CH_3OH) to yield four fractions (Fr. 1J1 to Fr. 1J4). Fr. 1J2 (57.27 mg) was separated by MPLC to produce two subfractions (Fr. 1J2A and Fr. 1J2B). Fr. 1J2A (12.30 mg) was separated by semipreparative HPLC (CH_3OH/H_2O, 43∶57, 3 $mL{\cdot}min^{-1}$) to obtain **17** (3.40 mg, t_R 25.9 min) and **15** (6.40 mg, t_R 30.2 min). Fr. 1J4 (661.19 mg) was separated by preparative HPLC (CH_3OH/H_2O–0.1% FA, 39∶61 to 74∶26, 10 $mL{\cdot}min^{-1}$) to yield **4** (7.10 mg, t_R 44.0 min) and **5** (2.45 mg, t_R 32.5 min).

Fr. 1K (6.06 g) was subjected to a Sephadex LH-20 column (CH_3OH) to generate four fractions (Fr. 1K1 to Fr. 1K4). Fr. 1K3 (1.46 g) was fractionated through a Sephadex LH-20 column (CH_3OH/H_2O, 9∶1) to generate three fractions (Fr. 1K3A to Fr. 1K3C).

Fr. 1K3C (63.70 mg) underwent purification *via* HPLC (CH_3CN/H_2O, 18∶82, 3 $mL{\cdot}min^{-1}$) to yield **14** (16.77 mg, t_R 21.2 min). Fr. 1K3A (956.90 mg) was fractionated by MPLC into four portions (Fr. 1K3A1 to Fr. 1K3A4). Fr. 1K3A1 (25.00 mg) was further purified through semipreparative HPLC (CH_3OH/H_2O, 39∶61 to 46∶54, 3 $mL{\cdot}min^{-1}$) to obtain **1** (13.50 mg, t_R 26.3 min). Fr. 1K3A2 (149.00 mg) underwent semipreparative HPLC (CH_3CN/H_2O, 33∶67, 3 $mL{\cdot}min^{-1}$) to produce **21** (39.97 mg, t_R 10.7 min) and **24** (70.32 mg, t_R 16.0 min). Fr. 1K3A3 (132.90 mg) was purified using semipreparative HPLC (CH_3CN/H_2O, 31∶69, 3 $mL{\cdot}min^{-1}$) to yield **22** (1.79 mg, t_R 45.0 min), **23** (39.17 mg, t_R 21.0 min), **25** (3.59 mg, t_R 34.0 min) and **26** (5.34 mg, t_R 23.0 min). Fr. 1K3A4 (1.66 g) was separated using a Sephadex LH-20 column (CH_3OH/H_2O, 9∶1) to generate four fractions (Fr. 1K3A4A to Fr. 1K3A4D). Fr. 1K3A4A (102.30 mg) underwent semipreparative HPLC (CH_3OH/H_2O, 26∶74, 3 $mL{\cdot}min^{-1}$) to yield **7** (5.12 mg, t_R 35.0 min). Fr. 1K3A4B (1.17 g) was purified through semipreparative HPLC (CH_3OH/H_2O, 35∶65, 3 $mL{\cdot}min^{-1}$) to obtain **6** (14.30 mg, t_R 32.7 min). Fr. 1K3A4C (308.00 mg) was fractionated by MPLC into two portions (Fr. 1K3A4C1 and Fr. 1K3A4C2). Fr. 1K3A4C2 (27.10 mg) underwent semipreparative HPLC (CH_3CN/H_2O, 24∶76, 3 $mL{\cdot}min^{-1}$) to yield **16** (16.50 mg, t_R

55.0 min).

3.5. Spectral data of compounds **1**–**7** and **26**–**27**

Auxarthrolone A (**1**): colorless crystal; $[\alpha]_D^{20}$ −112 (*c* 0.41, MeOH); UV (MeOH) λ_{max} (log ε) 198 (3.09), 242 (2.75), 291 (2.44), 339 (2.37) nm; IR ν_{max} 3415, 1747, 1641, 1616, 1382 cm^{-1}; ECD (MeOH) λ_{max} ($\Delta\varepsilon$) 250 (+2.29), 293 (+0.85), 335 (−4.99) nm; ^{1}H NMR data (700 MHz, acetone-d_6) and ^{13}C NMR data (175 MHz, acetone-d_6), see Tables 1 and 2; HR-ESI-MS *m/z* 397.1134 $[M + H]^+$ (Calcd. for $C_{18}H_{21}O_{10}$, 397.1130).

Auxarthrolone B (**2**): yellow solid; $[\alpha]_D^{20}$ +3 (*c* 0.04, MeOH); UV (MeOH) λ_{max} (log ε) 198 (3.46), 221 (3.03), 288 (2.89), 331 (2.71) nm; IR ν_{max} 3412, 1624, 1375 cm^{-1}; ECD (MeOH) λ_{max} ($\Delta\varepsilon$) 217 (−0.55), 244 (+0.09), 293 (+0.18), 329 (+0.18) nm; ^{1}H NMR data (600 MHz, acetone-d_6) and ^{13}C NMR data (150 MHz, acetone-d_6), see Tables 1 and 2; HR-ESI-MS *m/z* 371.1340 $[M + H]^+$ (Calcd. for $C_{17}H_{23}O_9$, 371.1337).

Auxarthrolone C (**3**): yellow solid; $[\alpha]_D^{20}$ −95 (*c* 0.1, MeOH); UV (MeOH) λ_{max} (log ε) 199 (3.06), 216 (2.70), 287 (2.55), 327 (2.31) nm; IR ν_{max} 3357, 1626, 1435, 1377, 1027 cm^{-1}; ECD (MeOH) λ_{max} ($\Delta\varepsilon$) 216 (+2.46), 244 (+6.13) nm; ^{1}H NMR data (600 MHz, acetone-d_6) and ^{13}C NMR data (150 MHz, acetone-d_6), see Tables 1 and 2; HR-ESI-MS *m/z* 341.1236 $[M + H]^+$ (Calcd. for $C_{16}H_{21}O_8$, 341.1231).

Auxarthrolone D (**4**): light yellow crystal; $[\alpha]_D^{20}$ +76 (*c* 0.24, MeOH); UV (MeOH) λ_{max} (log ε) 199 (3.10), 217 (2.64), 237 (2.40), 289 (2.61), 330 (2.31) nm; IR ν_{max} 3360, 1804, 1623, 1576, 1373 cm^{-1}; ECD (MeOH) λ_{max} ($\Delta\varepsilon$) 222 (+1.33), 239 (+2.08) nm; ^{1}H NMR data (700 MHz, acetone-d_6) and ^{13}C NMR data (175 MHz, acetone-d_6), see Tables 1 and 2; HR-ESI-MS *m/z* 367.1026 $[M + H]^+$ (Calcd. for $C_{17}H_{19}O_9$, 367.1024).

Auxarthrolone E (**5**): yellow solid; $[\alpha]_D^{20}$ +9 (*c* 0.04, MeOH); UV (MeOH) λ_{max} (log ε) 198 (2.90), 217 (2.50), 236 (2.26), 288 (2.43), 328 (2.20) nm; IR ν_{max} 3515, 2974, 1626, 1579, 1378, 1300, 1209, 1160 cm^{-1}; ECD (MeOH, *c* 0.1) λ_{max} ($\Delta\varepsilon$) 213 (−4.43), 244 (+0.73), 286 (+4.06), 317 (−3.10), 347 (+1.00) nm; ^{1}H NMR data (700 MHz, methanol-d_4) and ^{13}C NMR data (175 MHz, methanol-d_4), see Tables 2 and 3; HR-ESI-MS *m/z* 323.1127 $[M + H]^+$ (Calcd. for $C_{16}H_{19}O_7$, 323.1126).

Auxarthrolone F (**6**): light red solid; $[\alpha]_D^{20}$ +102 (*c* 0.41, MeOH); UV (MeOH) λ_{max} (log ε) 198 (3.30), 220 (2.90), 276 (2.54) nm; IR ν_{max} 3420, 1687, 1617, 1583, 1441, 1329 cm^{-1}; ECD (MeOH) λ_{max} ($\Delta\varepsilon$) 273 (−5.87), 331 (+4.79) nm; ^{1}H NMR data (700 MHz, acetone-d_6) and ^{13}C NMR data (175 MHz, acetone-d_6), see Tables 2 and 3; HR-ESI-MS *m/z* 339.1074 $[M + H]^+$ (Calcd. for $C_{16}H_{19}O_8$, 339.1075).

Auxarthrolone G (**7**): yellow solid; $[\alpha]_D^{20}$ +12 (*c* 0.34, MeOH); UV (MeOH) λ_{max} (log ε) 200 (3.19), 227 (2.48), 293 (2.15) nm; IR ν_{max} 3395, 1729, 1679, 1608, 1499 cm^{-1}; ECD (MeOH) λ_{max} ($\Delta\varepsilon$) 212 (+3.85), 239 (−1.74) nm; ^{1}H NMR data (600, acetone-d_6) and ^{13}C NMR data (150 MHz, acetone-d_6), see Tables 2 and 3; HR-ESI-MS *m/z* 409.1105 $[M + Na]^+$ (Calcd. for $C_{17}H_{22}O_{10}Na$, 409.1106).

Malfilamentoside E (**26**): white powder; $[\alpha]_D^{20}$ +31.0 (*c* 0.04, MeOH); UV (MeOH) λ_{max} (log ε) 199 (2.58), 257 (1.75) nm; IR ν_{max} 3317, 1775, 1633, 1540, 787, 701 cm^{-1}; ECD (MeOH) λ_{max} ($\Delta\varepsilon$) 242 (−2.17) nm; ^{1}H NMR data (600 and 700 MHz, acetone-d_6 and DMSO-d_6) and ^{13}C NMR data (150 and 175 MHz, acetone-d_6 and DMSO-d_6), see Table 4; HR-ESI-MS *m/z* 470.1821 $[M + H]^+$ (Calcd. for $C_{25}H_{28}O_8N$, 470.1809).

Auxarthrolide A (**27**): yellow solid; $[\alpha]_D^{20}$ −37.8 (*c* 0.12, MeOH); UV (MeOH) λ_{max} (log ε)199 (3.05), 259 (2.24) nm; IR ν_{max} 3357, 1758, 1613, 1597, 1514, 800, 750, 700 cm^{-1}; ECD (MeOH, *c* 0.1) λ_{max} ($\Delta\varepsilon$) 221 (+0.81), 257 (−1.92) nm; ^{1}H NMR data (700 MHz, methanol-d_4) and ^{13}C NMR data (175 MHz, methanol-d_4), see Table 4; HR-ESI-MS *m/z* 283.0971 $[M + H]^+$ (calcd for $C_{17}H_{15}O_4$, 283.0965).

3.6. Determination of absolute configuration of the sugar moiety

Acid hydrolysis of **26** was conducted according to established literature [31]. Compound **26** (0.50 mg) was dissolved in MeOH (1.0 mL), and 2 mol·L^{-1} HCl (1.0 mL) was added to the CH_3OH-solution. The solution underwent heating at 70 °C for 10 h. Following MeOH and HCl evaporation, the resulting mixture was diluted with H_2O (1.0 mL) and extracted with EtOAc (1.0 mL × 3) to obtain the EtOAc-soluble extraction and H_2O-soluble extraction. The H_2O-soluble extraction underwent evaporation and drying *in vacuo*, followed by dissolution in pyridine (1.0 mL). Subsequently, 1.00 mg of L-cysteine methyl ester hydrochloride was added. The mixture was maintained at 60 °C for 2.5 h. After solvent removal under reduced pressure and drying *in vacuo*, *N*-trimethylsilylimidazole (TSIM) (0.2 mL) was added to the resulting mixture for 2.5 h at 60 °C. The mixture underwent partitioning between *n*-hexane and H_2O (1.0 mL each), and the obtained *n*-hexane extract was analyzed by GC-QTOF. The derivative of standard D-glucosamine was prepared identically. The extracted ion chromatograms at *m/z* 362.1 of the derivatives of the sugar moiety of **26** and standard D-glucosamine in positive ion mode exhibited identical retention times at 15.523 min (Fig. S14).

3.7. Quantum chemical calculations of **2**, **3**, **5**–**7**, **26** and **27**

The quantum chemical calculation methods followed previously reported procedures [32]. The Gaussian 16 software (Gaussian, Inc., USA) and SYBYL-X 2.0 program (Tripos, Inc., USA) were utilized for theoretical calculations. Random conformational searches of compounds **1**, **2**, **3**, **5**–**7**, **26** and **27** were performed using a MMFF94s molecular force field within 6 kcal·mol^{-1} energy, yielding corresponding conformers. Further optimization of these conformers was calculated at the B3LYP/6-31G(d) level. Subsequently, ^{1}H and ^{13}C NMR chemical calculations employed the GIAO method at the mPW1PW91/6-31 + G(d, p) level with the PCM model in acetone or methanol. The DP4+ probability analysis [33–34] was applied to assign the corrective stereoisomer. ECD calculations were performed at the B3LYP/6-31 + G(d, p) level with the PCM model in methanol. Boltzmann distribution parameters determined the proportion of each conformer.

3.8. X-ray crystallography analysis

Suitable crystals of **1** and **4** were collected on a XtaLAB Synergy four-circle diffractometer (Rigaku, Americas) equipped with Cu Kα radiation (λ = 1.541 78 Å). The structures and absolute configurations of **1** and **4** were solved and determined with the ShelXT28 program (George M. Sheldrick, Germany) using Intrinsic Phasing. Crystallographic data for **1** and **4** were deposited in the Cambridge Crystallographic Data Centre with Deposition Nos. CCDC 2314022 and 2314021, respectively, which could be obtained free of charge from the CCDC *via* https://www.ccdc.cam.ac.uk/structures/.

Crystal data for **1**: $C_{18}H_{20}O_{10}{\cdot}2CH_3OH$, *Mr* = 460.42, *a* = 7.9406 (2) Å, *b* = 8.5959 (2) Å, *c* = 32.4443 (6) Å, α = 90 °, β = 90 °, γ = 90 °, *V* = 2214.5 (1) $Å^3$, *T* = 304 K, space group $P2_12_12_1$, *Z* = 4, μ(Cu Kα) = 0.987 mm^{-1}, 123 04 reflections collected in the range of 5.448° ≤ 2θ ≤ 152.526°, 4315 independent reflections (R_{int} = 0.0369, R_{sigma} = 0.0331). The final R_1 values were 0.0374 [$I > 2\sigma(I)$]. The final wR_2 values were 0.1037 [$I > 2\sigma(I)$]. The final R_1 values were 0.0404 (all data). The final wR_2 values were 0.1057 (all data). The goodness of fit on F^2 was 1.148. Flack parameter = −0.15 (9). CCDC: 2314022.

Crystal data for **4**: $C_{17}H_{18}O_9$, *Mr* = 366.31, *a* = 19.8495 (7) Å, *b* = 13.2704 (5) Å, *c* = 6.1764 (2) Å, α = 90 °, β = 90 °, γ = 90 °, *V* =

1626.9 (1) Å^3, T = 303.1 (2) K, space group $P2_12_12_1$, Z = 4, μ(Cu Kα) = 1.051 mm^{-1}, 8790 reflections collected in the range of 8.014° ≤ 2θ ≤ 152.782°, 3019 independent reflections (R_{int} = 0.0369, R_{sigma} = 0.0335). The final R_1 values were 0.0380 [$I > 2\sigma$ (I)]. The final wR_2 values were 0.1038 [$I > 2\sigma$ (I)]. The final R_1 values were 0.0441 (all data). The final wR_2 values were 0.1083 (all data). The goodness of fit on F^2 was 1.059. Flack parameter = −0.10 (13). CCDC: 2314021.

3.9. Cytotoxic bioassay

The cytotoxicity of compounds **1**–**27** was evaluated against two human cancer cell lines (U87MG and U251MG) using the cell counting kit-8 (CCK8) method as previously described [35]. Cell lines in DMEM with 10% fetal bovine serum (FBS, BI) were seeded in 96-well cell culture plates and incubated overnight in a humidified atmosphere (37 °C, 5% CO_2). Subsequently, cells underwent treatment with various concentrations of test compounds for 24 h, followed by CCK8 solution addition to each well and 1 h incubation. The formed formazan crystals were dissolved in DMSO, and OD measurements were taken at 450 nm using a microplate reader. Cell viability was assessed, and cytotoxic activity was calculated as IC_{50} value. The mean IC_{50} was determined from three independent experiments of duplication for each assay and similar determinations.

3.10. Fibroblast proliferation assay

NIH3T3 cells were seeded at 6000 cells/well in 96-well plates and cultured in DMEM supplemented with 10% serum for 24 h at 37 °C, 5% CO_2. Subsequently, the medium containing 10% serum was replaced with a serum-free medium. The control group was maintained for 24 h in a 5% CO_2 incubator at 37 °C. For the experimental groups, 0.20 mmol·L^{-1} oleic acid was added to the OA group, while 0.20 mmol·L^{-1} oleic acid and varying concentrations (0.1, 1.0, 10.0 μmol·L^{-1}) of compounds dissolved in DMSO were added to the treatment group. Each concentration was tested in triplicate. The OA group and treatment group were incubated for 24 h at 37 °C, 5% CO_2. After incubation, the supernatant was removed, and CCK8 (100 μL, diluted 10-fold with DMEM) was added to each well. Following 0.5–2 h incubation at 37 °C, absorbance at 450 nm was measured using a Molecular Devices SpectraMax M5 (USA).

4. Conclusions

In summary, nine novel secondary metabolites were isolated from *A. umbrinum* DSM3193, comprising seven tetrahydroanthraquinones (**1**–**7**), one γ-butenolide glucoside (**26**), one γ-butanolide (**27**), and eighteen known compounds. The structures of these compounds were fully characterized. Compounds **10** and **14** demonstrated moderate cytotoxicity against U87 and U251 cell lines. Additionally, compounds **1**, **14**, **15**, and **17** showed fibroblast proliferation-promoting activity.

Funding

This work was supported by the National Key Research and Development Program of China (No. 2018YFA0901900) and the National Science Fund for Distinguished Young Scholars (No. 82225042).

Availability of supporting information

Supplementary data for this article can be obtained by sending an E-mail to corresponding authors. The data include: 1D and 2D NMR, HR-ESI-MS, UV, and IR spectra of compounds **1**–**7** and **26**–**27**; the details of quantum chemical calculations, such as the results of DP4+ analysis of **1**–**3**, **5**, **6** and **26**, the calculated and experimental NMR data of **1**–**3**, **5**, **6** and **26**, and calculated and experimental ECD spectra of **1**–**3**, **5**–**7**, **26** and **27** (PDF); and crystallographic data for **1** (CIF) and **4** (CIF).

Declaration of competing interest

These authors have no conflict of interest to declare.

References

1 Du FX, Guo XM, Yang L, et al. Natural medicinal products of fungal origin. *Microbiol China*. 2019;46(9):2411-2418. https://doi.org/10.13344/j.microbiol.china.180928.
2 Li S, Li Z, Qian L, et al. Fumigaclavine I, a new alkaloid isolated from endophyte *Aspergillus Terreus*. *Chin J Nat Med*. 2015;13(12):937-941. https://doi.org/10.1016/S1875-5364(15)30101-1.
3 Luo ZW, Yin FC, Kong LY, et al. Progress in approved drugs from natural product resources. *Chin J Nat Med*. 2024;22(3):195-211. https://doi.org/10.1016/S1875-5364(24)60582-0.
4 Zhong BF, Wan J, Shang CH, et al. Biosynthesis of rumbrins and inspiration for discovery of HIV inhibitors. *Acta Pharm Sin B*. 2022;12(11):4193-4203. https://doi.org/10.1016/j.apsb.2022.02.005.
5 Isaka M, Chinthanom P, Rachtawee P, et al. Cytotoxic hydroanthraquinones from the mangrove-derived fungus *Paradictyoarthrinium diffractum* BCC 8704. *J Antibiot (Tokyo)*. 2015;68(5):334-338. https://doi.org/10.1038/ja.2014.153.
6 Clark B, Capon RJ, Lacey E, et al. Roquefortine E, a diketopiperazine from an Australian isolate of *Gymnoascus reessii*. *J Nat Prod*. 2005;68(11):1661-1664. https://doi.org/10.1021/np0503101.
7 Miyashita K, Yagi T, Kagaya N, et al. Identification of compounds that preferentially suppress the growth of T-cell acute lymphoblastic leukemia-derived cells. *Cancer Sci*. 2023;114(10):4032-4040. https://doi.org/10.1111/cas.15918.
8 Elsebai MF, Rempel V, Schnakenburg G, et al. Identification of a potent and selective cannabinoid CB 1 receptor antagonist from *Auxarthron reticulatum*. *ACS Med Chem Lett*. 2011;2(11):866-869. https://doi.org/10.1021/ml200183z.
9 Rangel-Grimaldo M, Macías-Rubalcava ML, González-Andrade M, et al. α-Glucosidase and protein tyrosine phosphatase 1B inhibitors from *Malbranchea circinata*. *J Nat Prod*. 2020;83(3):675-683. https://doi.org/10.1021/acs.jnatprod.9b01108.
10 Xu HX, Yang T, Zhang LP, et al. Ocauxarthrol A from *Auxarthron umbrinum* SCSIO 40432 and configurational reassignment of chrysoqueen and auxarthrols. *Tetrahedron Lett*. 2021;66:152842. https://doi.org/10.1016/j.tetlet.2021.152842.
11 Yamagishi Y, Matsuoka M, Odagawa A, et al. A new cytoprotective substanci produced by *Auxarthron umbrinum* I. Taxonomy, production, isolation and biological activities. *J Antibiot (Tokyo)*. 1993;46(6):884-887. https://doi.org/10.7164/antibiotics.46.884.
12 Xu H, Wang L, Zhang L, et al. Configurational assignment of malfilamentoside A and a new furanone glycoside malfilamentoside D. *Chin J Org Chem*. 2022;42(4):1229-1234. https://doi.org/10.6023/cjoc202110038.
13 Gerke J, Bayram Ö, Feussner K, et al. Breaking the silence: protein stabilization uncovers silenced biosynthetic gene clusters in the fungus *Aspergillus Nidulans*. *Appl Environ Microbiol*. 2012;78(23): 8234-8244. https://doi.org/10.1128/AEM.01808-12.
14 Entwistle R, Bruno KS. Molecular genetic analysis reveals that a nonribosomal peptide synthetase-like (NRPS-like) gene in *Aspergillus nidulans* isresponsible for microperfuranone biosynthesis. *Appl Microbiol Biotechnol*. 2013;96(3):739-748. https://doi.org/10.1007/s00253-012-4098-9.
15 Dong G, Chen ZL, Yan S, et al. Steroids and dihydroisocoumarin glycosides from *Xylaria* sp. by the one strain many compounds strategy and their bioactivities. *Chin J Nat Med*. 2023;21;(2):154-160. https://doi.org/10.1016/S1875-5364(23)60394-2.
16 Bode HB, Bethe B, Höfs R, et al. Big effects from small changes: possible ways to explore nature's chemical diversity. *Chem Bio Chem*. 2002;3(7):619-627. https://doi.org/10.1002/1439-7633(20020703)3:7<619::AID-CBIC619>3.0.CO;2-9.
17 Alvi KA, Rabenstein J. Auxarthrol A and auxarthrol B: two new tetrahydoanthraquinones from *Auxarthron umbrinum*. *J Ind Microbiol Biotechnol*. 2004;31(1):11-15. https://doi.org/10.1007/s10295-003-0106-5.
18 Ge X, Sun C, Feng Y, et al. Anthraquinone derivatives from a marine-derived fungus *Sporendonema casei* HDN16-802. *Mar Drugs*. 2019;17(6):334. https://doi.org/10.3390/md17060334.
19 Ivanova VB, Hoshino Y, Yazawa K, et al. Isolation and structure elucidation of two new antibacterial compounds produced by *Chrysosporium queenslandicum*. *J Antibiot (Tokyo)*. 2002;55(10):914-918. https://doi.org/10.7164/antibiotics.55.914.
20 Matsumori N, Kaneno D, Murata M, et al. Stereochemical determination of acyclic structures based on carbon-proton spin-coupling constants. A method of configuration analysis for natural products. *J Org Chem*. 1999;64(3):866-876. https://doi.org/10.1021/jo981810k.
21 Yan HJ, Li XM, Li CS, et al. Alkaloid and anthraquinone derivatives produced by the marine-derived endophytic fungus *Eurotium rubrum*. *Helv Chim Acta*. 2012;95(1):163-168. https://doi.org/10.1002/hlca.201100255.

22 Lauro G, Das P, Riccio R, et al. DFT/NMR Approach for the configuration assignment of groups of stereoisomers by the combination and comparison of experimental and predicted sets of data. *J Org Chem*. 2020;85(5):3297-3306. https://doi.org/10.1021/acs.joc.9b03129.
23 Kim JW, Son S, Kim GS, et al. Aromatic butenolides produced by a soil ascomycete *Auxarthron* sp. KCB15F070 derived from a volcanic island. *Tetrahedron Lett*. 2019;60(45):151227. https://doi.org/10.1016/j.tetlet.2019.151227.
24 Gill M, Smrdel AF, Strauch RJ, et al. Pigments of fungi. Part 12. Structure and absolute stereochemistry of antibiotic tetrahydroanthraquinones from the fungus *Dermocybe splendida* Horak. X-Ray structure determination of austrocortirubin phenylboronate and austrocortilutein acetonide. *J Chem Soc Perkin Transact*. 1990;1:1583. https://doi.org/10.1039/p19900001583.
25 Jiang HL, Luo XH, Wang XZ, et al. New isocoumarins and alkaloid from Chinese insect medicine, *Eupolyphaga Sinensis* Walker. *Fitoterapia*. 2012;83(7):1275-1280. https://doi.org/10.1016/j.fitote.2012.06.005.
26 Khamthong N, Rukachaisirikul V, Tadpetch K, et al. Tetrahydroanthraquinone and xanthone derivatives from the marine-derived fungus *Trichoderma aureoviride* PSU-F95. *Arch Pharm Res*. 2012;35(3):461-468. https://doi.org/10.1007/s12272-012-0309-2.
27 Hosoe T, Iizuka T, Komai SI, et al. 4-Benzyl-3-phenyl-5*H*-furan-2-one, a vasodilator isolated from *Malbranchea filamentosa* IFM 41300. *Phytochemistry*. 2005;66(23):2776-2779. https://doi.org/10.1016/j.phytochem.2005.08.014.
28 Lin Y, Li H, Jiang G, et al. A novel *γ*-lactone, eutypoid-A and other metabolites from marine fungus *Eutypa* sp. (#424) from the South China Sea. *Indian J Chem*. 2002;41(7):1542-1544. https://doi.org/10.1002/chin.200245200.
29 Parker AN, Lock MJ, Hutchison JM, et al. Synthesis of 4-benzyl-3-phenylbutenolide natural products. *Tetrahedron Lett*. 2013;54(39):5322-5324. https://doi.org/10.1016/j.tetlet.2013.07.101.
30 Wakana D, Hosoe T, Itabashi T, et al. Two new furanone glycosides, malfilamentosides A and B, from *Malbranchea filamentosa*. *Mycotoxins*. 2008;58(1):1-6. https://doi.org/10.2520/myco.58.1.
31 Chen K, Zhou J, Dun B, et al. Onygenaleosides A–F, 6/5 bicyclic ring skeleton triterpene glycosides with insecticidal activity from *Onygenales* sp. YX1425. *J Nat Prod*. 2023;86(12):2621-2629. https://doi.org/10.1021/acs.jnatprod.3c00243.
32 Jiao SG, Huang H, Wang L, et al. Alashanines A–C, three quinone-terpenoid alkaloids from *Syringa pinnatifolia* with cytotoxic potential by activation of ERK. *J Org Chem*. 2023;88(11):7096-7103. https://doi.org/10.1021/acs.joc.3c00369.
33 Grimblat N, Zanardi MM, Sarotti AM. Beyond DP4: an improved probability for the stereochemical assignment of isomeric compounds using quantum chemical calculations of NMR shifts. *J Org Chem*. 2015;80(24):12526-12534. https://doi.org/10.1021/acs.joc.5b02396.
34 Zanardi MM, Sarotti AM. Sensitivity analysis of DP4+ with the probability distribution terms: development of a universal and customizable method. *J Org Chem*. 2021;86(12):8544-8548. https://doi.org/10.1021/acs.joc.1c00987.
35 Ren LW, Li W, Zheng XJ, et al. Benzimidazoles induce concurrent apoptosis and pyroptosis of human glioblastoma cells *via* arresting cell cycle. *Acta Pharmacol Sin*. 2022;43(1):194-208. https://doi.org/10.1038/s41401-021-00752-y.